Check for updates

Chemistry-A European Journal



www.chemeurj.org

Recent Advances in MOF—Based Dual—Atom Catalysts for CO₂ Reduction

Wen-Jie Shi^[a] and Tong-Bu Lu*^[a]

In recent years, the development of efficient catalysts for photo-/electro-catalytic CO₂ reduction reaction (CO₂RR) has become a major research focus due to growing environmental concerns and energy demands. Dual—atom catalysts (DACs), composed of two metal atoms with suitable metal-metal distance integrated into the supports, have shown great promise in enhancing catalytic performance via the dual-metal synergistic catalysis (DMSC) effect. This review highlights the advancements in Metal-organic framework (MOF)-based DACs, which combine the high atomic efficiency of DACs with tunable and defined structures and high metal loadings. In this review, we summarized the recent developments on the synthesis strategies of MOF-based DACs and their applications in CO₂RR, focusing on the role of DMSC effect in improving catalytic activity, stability, and selectivity. Additionally, we also discuss the influence of the local electronic structure, coordination environment, and metal atom interactions on catalytic performance. This review aims to provide a comprehensive understanding of MOF-based DACs and offers insights into their future potential in sustainable energy conversion.

1. Introduction

The world is facing a critical point in energy development due to the heavy reliance on fossil fuels, rising energy consumption, and increasing environmental concerns.^[1-5] As a result, the development of efficient energy conversion technologies has become an active research area. Many of these technologies rely on effective catalysis, which is crucial for enabling the large-scale adoption of sustainable energy, reducing energy consumption, and lowering costs.^[6-8] Among these technologies, photocatalytic and electrocatalytic CO₂ reduction has attracted significant attention. [9,10] However, to achieve efficient photocatalytic and electrocatalytic CO2 reduction, there is an urgent need for advanced catalysts that can provide both high performance and long-term stability.

Dual—atom catalysts (DACs) with two metal atoms precisely incorporated into support materials, offer a unique advantage in enhancing catalytic performance through dual metal synergistic catalysis (DMSC) effect.^[11] Unlike single—atom catalysts (SACs) [12-14] or traditional metal nanoparticles catalysts, [15,16] DACs display unique features such as dual atom synergy facilitating the reactant activation, accelerating charge transfer, reducing activation energy, etc., which induce the dual-atom sites with excellent activity and stability in catalysis.[17-19] The combination of high atomic efficiency and cooperative metal interactions has driven significant research interest. However, despite their promising catalytic activity, the complexity of optimizing dual-metal sites for specific reactions can present challenges in their design and scalability.

[a] W.-J. Shi, T.-B. Lu

Institute for New Energy Materials & Low Carbon Technologies, School of Material Science & Engineering, Tianjin University of Technology, Tianjin 300384, China

E-mail: lutongbu@tjut.edu.cn

Metal—organic frameworks (MOFs), [20-23] which are crystalline porous materials made up of metal nodes and organic linkers, have emerged as a promising support for DACs. The ordered arrangement of metal nodes and ligands in MOFs offers several advantages, including high metal loadings, tunable porous structures, and customizable catalytic sites. Recent advancements have demonstrated that MOF-based DACs can significantly enhance reaction activity, selectivity, and stability in various energy conversion reactions.[24-27] However, the specific applications of MOF-based DACs in photocatalytic and electrocatalytic CO₂RR have not been thoroughly explored in recent literature. This review aims to fill this gap by comprehensively summarizing recent progress in the synthesis and application of MOF-based DACs, with a particular focus on their critical role in photocatalytic and electrocatalytic CO₂RR. Additionally, the review delves into the DMSC effect, examining its influence on catalytic performance through local electronic structure, coordination environment, and metal atom interactions. This discussion provides essential insights for the development of next-generation catalysts and paves the way for the practical implementation of MOF-based DACs in sustainable energy technologies.

2. Synthesis Strategies

Several strategies for design and synthesis of MOF-based DACs have been developed in recent years, including: 1) using metal nodes in MOFs, 2) employing surface modification to introduce metal sites, and 3) coordinating dual metals with ligands in MOFs. This review systematically summarizes recent progress in using MOF precursors and templates to create well-dispersed DACs. Additionally, the synthesis mechanisms and typical examples of each strategy are discussed.

As the main component, metal ions in the secondary building units (SBUs) of MOFs are periodically dispersed within the

Chemistry Europe

European Chemical Societies Publishing

Review doi.org/10.1002/chem.202500636

MOF structure, enabling the precise positioning of dual-atom sites, and facilitating enhanced catalytic activity. This arrangement allows for optimal interactions between the metal atoms, which is crucial for improving reaction efficiency and stability in various catalytic processes. Lu et al. successfully synthesized two types of Ni-based MOF DACs with rich exposure of (100) and (010) crystal facets by adding NaOH solution during the solvothermal synthesis process (Figure 1a).^[28] Selected—area electron diffraction and high-resolution transmission electron microscopy images confirmed the presence of the main crystal facets, (100) and (010). The Ni-based MOF DACs with (100) crystal facets demonstrated powerful catalytic behavior for photocatalytic CO₂-to-CO conversion. This enhanced performance is attributed to the synergistic catalysis between two neighboring Ni sites, which are separated by a close distance of 3.50 Å on the surface of the Ni-based MOF DACs with (100) crystal facets. This close separation significantly lowered the rate—determining free-energy change (ΔG), enhancing the overall reaction efficiency. Moreover, An et al. reported the synthesis of Fe/Co DACs using the solvothermal method to prepare MIL-101(Fe, Co). [29] This involved adding Co(NO₃)₂·6H₂O to a mixed solution of FeCl₃ and H₂BDC. Due to the higher electronegativity of Co (1.88) compared to Fe (1.83), the introduction of Co atoms into MIL—101(Fe) decreased the valence electron density around Fe from 4.56 e-Å⁻³ to 4.45 e-Å⁻³. This change facilitated electron transfer from Fe to Co centers through Fe-O-Co bonds, resulting in the Co atoms in MIL-101(Fe, Co) having the highest valence electron density of 5.35 e-Å⁻³. As a result, MIL-101(Fe, Co) exhibited enhanced catalytic performance.

Surface modification of MOFs also plays a crucial role in constructing these dual—atom sites, further enhancing the multifunctionality and catalytic properties of MOF-based materials. For instance, Zhong et al. used flexible ethylene diamine tetraacetic acid (EDTA) as a modifier on the SBUs of MOF-808 and then treated the functionalized MOF-808 with Cu and Ni metal salts [30] (Figure 1b). The Cu and Ni dual—metal sites were successfully incorporated into the robust MOF-808, resulting in a bioinspired MOF-808-CuNi photocatalyst for CO₂-to-CH₄ conversion. X-ray absorption near-edge structure analysis confirmed that both Cu and Ni species were in their single-site forms and four-coordinated with two N and two O atoms from EDTA. The Cu/Ni DACs showed higher CH₄ production than the corresponding single-metal MOF-808-Cu and MOF-808-Ni catalysts. Density functional theory (DFT) calculations revealed that the synergistic effect and self-adaptive behavior between Cu and Ni sites stabilized various C1 intermediates and suppressed the formation of undesired byproducts, leading to high CH₄ selectivity. These results pave the way for designing dual-metal species as precisely defined catalytically active sites above the SBUs of MOFs.

DACs can be synthesized through the modification of SBUs. However, the range of metals that can be used is limited due to restrictions in the metal nodes during MOF preparation, which hinders the development of MOF-based DACs. Fortunately, functional organic ligands offer significant advantages in coordinating with various metal ions, providing a strong anchoring effect that helps stabilize the dual-metal sites in MOF-based DACs. Our group synthesized an indium-based MOF (H₂L-In) by metallizing the macrocyclic ligand in H₂L-In with one or two metal ions in an ethanol solution [31] (Figure 2a). This process yielded three mononuclear metallic MOFs, three dinuclear homometallic MOFs, and three dinuclear heterometallic MOFs. In addition, Chen et al. employed postsynthetic modification (PSM) to fine-tune catalytic activity and precisely tailor the material properties and functions.[32] They first synthesized a conductive 2D π -conjugated MOF, Cu-HAB (HAB = hexaiminobenzene), which boasts an impressive electrical conductivity of 13 S cm⁻¹. This structure is constructed through the tripodal bridging of HAB ligands and planar Cu-N₄ nodes. Notably, the ligands in Cu-HAB remain protonated, indicating their ability to coordinate with additional metal ions. In this work, by applying PSM to Cu-HAB, they prepared a novel CuSn-HAB featuring unprecedented asymmetric or heterometallic Sn···Cu dual sites (Figure 2b), specifically SnN₂O₂ and CuN₄ sites bridged by μ -N atoms. The CuSn-HAB catalyst demonstrates excellent performance in the electrochemical CO₂RR for the selective production of ethanol.

In summary, the above strategies enable accurate control over metal site dispersion and coordination environments, significantly enhancing catalytic performance in CO₂ reduction



Dr. Wen-Jie Shi serves as an Associate Professor in New Energy Materials & Low Carbon Technologies at Tianjin University of Technology. She obtained her B.S. in Chemistry from Gannan Normal University in 2015 and her PhD in Inorganic Chemistry from Xiamen University in 2021, respectively. Her interests focus on the rational design and synthesis of functional MOF/COF-based catalysts for energy storage and conversion.



Prof. Tong-Bu Lu obtained his BS in 1988 and PhD in 1993 from Lanzhou University. After two years of post-doctoral fellowship at Sun Yat -- Sen University, he joined the faculty at the same university, and became a professor in 2000. In 2016, he moved to Tianjin University of Technology. His current research interests focus on the study of artificial photosynthesis, including the design of homogeneous and heterogeneous catalysts, especially DACs, for water splitting and CO₂ reduction.

15213765, 20

5, 28, Downloaded from https://chemistry-europe.onlinelibrary.wiley.com/doi/10.1002/chem.202500656 by Tanjin University Of, Wiley Online Library on [21/10/2025]. See the Terms and Conditions (https://onlinelibrary.wiley.com/errns-ad-conditions) on Wiley Online Library for rules of use; OA articles are governed by the applicable Cereative Commons. License

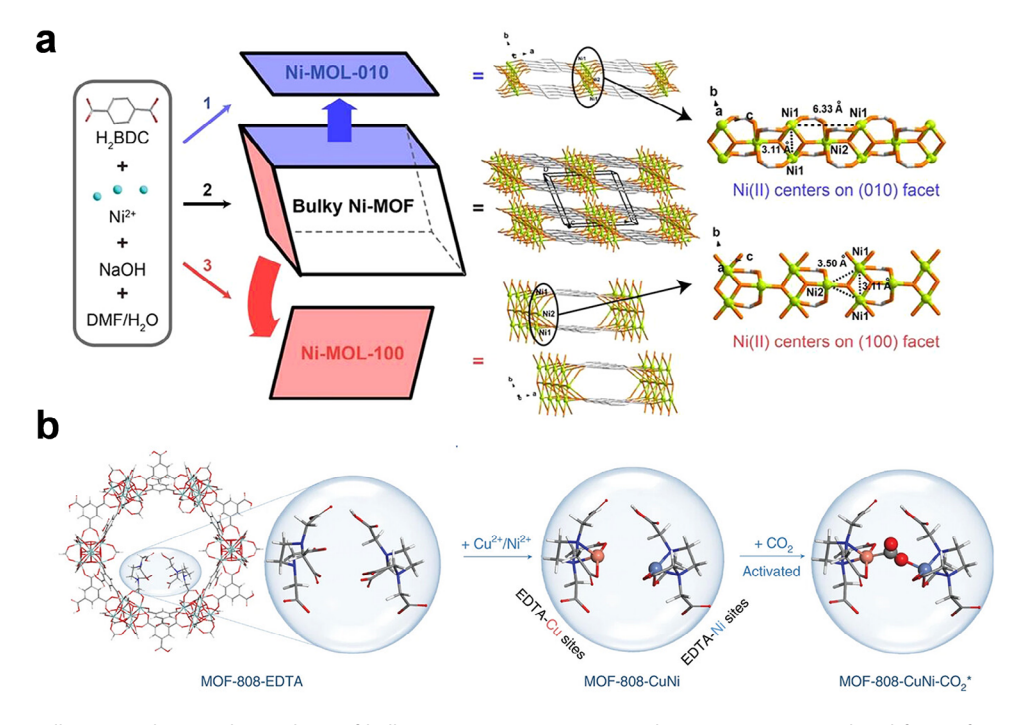


Figure 1. (a) Schematic illustration showing the synthesis of bulky Ni-MOF, Ni-MOL-010, and Ni-MOL-100. Reproduced from ref. 28 with permission from Wiley-VCH, Copyright 2021. (b) Schematic illustration of the implantation and self-adaption of flexible Cu/Ni dual-metal-site pairs in MOF-808 for highly selective CO₂ catalysis. Reproduced from ref. 30 with permission from Springer Nature, Copyright 2021.

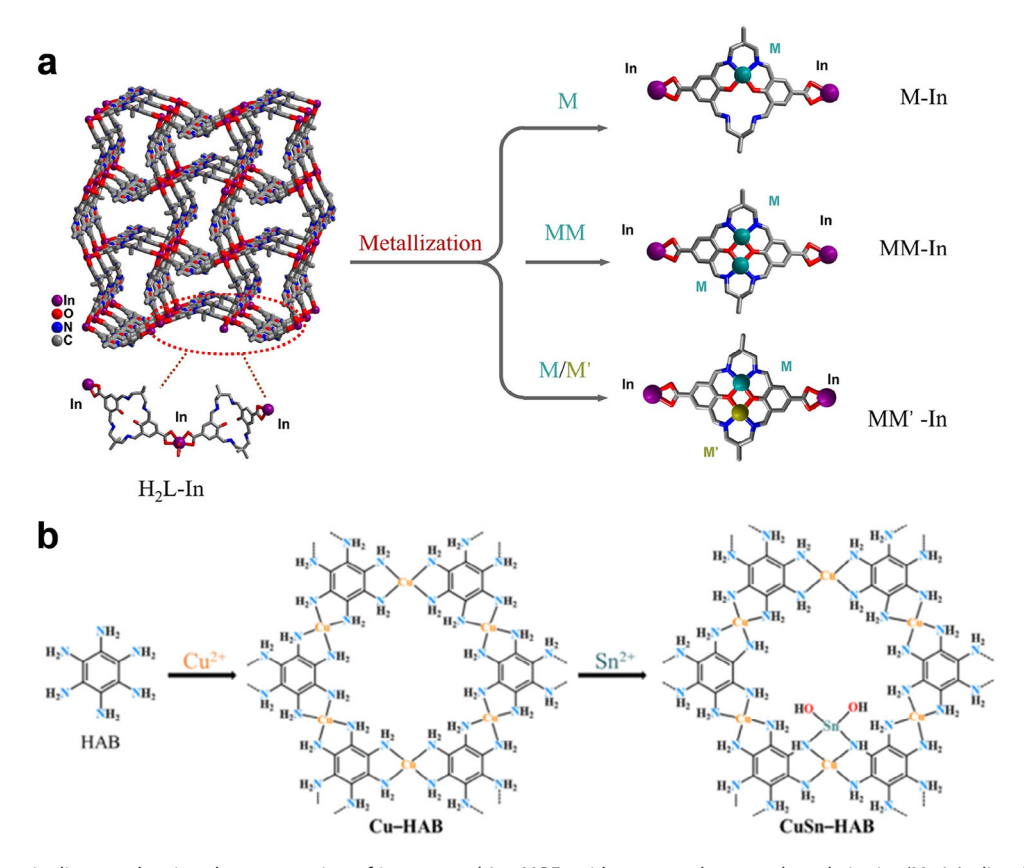


Figure 2. (a) Schematic diagram showing the construction of isostructural In-MOFs with mononuclear metal catalytic site (M-In), dinuclear homometallic catalytic site (MM-In), and dinuclear heterometallic catalytic site (MM'-In, M/M' = Co(II), Ni(II), Zn(II)). Reproduced from ref. 31 with permission from Springer Nature, Copyright 2024, (b) Illustration of the synthetic process for preparing CuSn-HAB. Reproduced from ref. 32 with permission from American Chemical Society, Copyright 2023.



Material	Light	Solution	PS ^[a] &SA ^[b]	Production rates	Ref.	
Ni-MOL-100	Xe lamp (300 mW, > 420 nm)	CH_3CN/H_2O (v:v = 4:1)	Ru(phen) ₃ (PF ₆) ₂ & TEOA ^[c]	CO: 11.89 \pm 0.65 mmol/g H $_2$: 0.47 \pm 0.10 mmol/g	[28]	
Ni-MOL-010	Xe lamp (300 mW, > 420 nm)	CH3CN/H2O (v:v = 4:1)	$Ru(phen)_3(PF_6)_2$ & TEOA $^{[c]}$	CO: 4.55 \pm 0.13 mmol/g	[28]	
Co ₂ -MOF(- NH ₂)	Xe lamp (300 mW, > 420 nm)	CH3CN/H2O (v:v = 4:1)	BIH ^[d]	CO: 2.44 mmol $g_{Co}^{-1} h^{-1}$	[33]	
MOF-808-CuNi	Xe lamp (300 mW, 760 nm $> \lambda >$ 420 nm)	CH3CN/TEOA/H2O (v:v:v = 3:1:1)	Ru(bpy) ₃ Cl ₂ ·6H ₂ O & TEOA ^[c]	CH ₄ : 158.7 umol g^{-1} h^{-1} CO: 2.3 umol g^{-1} h^{-1} HCOOH: 0 umol g^{-1} h^{-1} H ₂ : 1.7 umol g^{-1} h^{-1}	[30]	
CoZn—In	Xe lamp (300 mW, \geq 420 nm)	CH_3CN/H_2O (v:v = 3:2)	Ru(phen) ₃ (PF ₆) ₂ & TEOA ^[c] BIH ^[d]	CO: 12 700 umol $g^{-1} h^{-1}$ H_2 : 2020 umol $g^{-1} h^{-1}$	[31]	
CoNi–In	Xe lamp (300 mW, \geq 420 nm)	CH3CN/H2O (v:v = 3:2)	$Ru(phen)_3(PF_6)_2$ & $TEOA^{[c]}$ $BIH^{[d]}$	CO: 9219 umol $g^{-1} h^{-1}$ H_2 : 819 umol $g^{-1} h^{-1}$	[31]	
NiZn—In	Xe lamp (300 mW, \geq 420 nm)	CH3CN/H2O (v:v = 3:2)	Ru(phen) ₃ (PF ₆) ₂ & TEOA ^[c] BIH ^[d]	CO: 4616 umol g ⁻¹ h ⁻¹	[31]	

[[]a] PS: Photosensitizer.

reactions. Notably, close distance of dual—metal atoms (e.g., 3.50 Å in Ni—MOL—100) and precise control over coordination sites (e.g., Cu/Ni in MOF—808) are critical for catalytic selectivity and efficiency. Despite substantial advances, challenges such as limited metal compatibility still remain. Future research are suggested to focus on expanding applicable metals and developing novel ligand modifications to improve the practical applicability of MOF—based DACs for photocatalytic and electrocatalytic CO₂RR.

3. Photocatalytic CO₂ Reduction

Under this section, special emphasis is placed on reviewing the recent experimental findings of MOF—based DACs for photocatalytic CO₂RR. Specifically, the focus is on their ability to convert CO₂ into high—value products such as CO, methane, and formic acid. Additionally, the role of different metal combinations, including noble and transition metals, in enhancing photocatalytic performance is discussed. The photocatalytic CO₂ reduction performance over these catalysts is summarized in Table 1, highlighting key metrics such as reaction condition and production rates.

Homonuclear MOF—based DACs: Homonuclear MOF—based DACs consist of two identical metal atoms positioned within the MOF structure, allowing for the efficient exploitation of their synergistic effects. For example, our group synthesized Ni₂—based DACs and evaluated their photocatalytic CO₂ reduction performance $^{[28]}$ (Figure 3a). Among the catalysts tested, Ni—MOL—100 demonstrated the highest CO yield of 11.89 \pm 0.65 mmol/g with a CO selectivity of 96.2 \pm 0.6% (Table 1). These results highlight a significant improvement in catalytic efficiency compared to bulky Ni—MOF and Ni—MOL—010, which produced lower

CO yields of 2.62 \pm 0.10 and 4.55 \pm 0.13 mmol/g, respectively. The catalytic mechanism of Ni-MOL-100 in photochemical CO₂ reduction was investigated through fluorescence spectroscopy and DFT calculations. Fluorescence measurements revealed that during the photocatalytic CO₂ reduction process, the excited state of [Ru(phen)₃]²⁺ was quenched by Ni-MOL-100 via an oxidative quenching pathway, indicating rapid charge transfer between the excited state and the catalyst. This was further supported by the fact that Ni-MOL-100 exhibited a stronger fluorescence quenching ability compared to Ni-MOL-010 and bulky Ni-MOF, highlighting its superior catalytic activity. DFT calculations examined the reaction mechanism on both (010) and (100) crystal facets of Ni-MOL-100 (Figure 3b). It was found that CO₂ adsorption on the (100) facet is more favorable due to a stronger interaction between the Ni centers and CO2, resulting in a lower free energy change (ΔG) for the formation of the *COOH intermediate. The DMSC effect is facilitated by the close proximity of two Ni sites on the (100) facet, stabilizes the *COOH intermediate and promotes efficient CO2-to-CO conversion. The *CO intermediate is then formed and desorbed, with CO desorption being the rate-determining step. In comparison, the (010) facet exhibited a higher ΔG for *COOH formation, making CO₂ reduction less efficient. The findings demonstrate that the dinuclear metal sites in Ni-MOL-100 play a crucial role in enhancing the catalytic performance for photochemical CO₂ reduction. The synergistic effects of these metal sites, along with the favorable crystal facet and DMSC effect, result in the superior performance of Ni-MOL-100 for CO₂-to-CO conversion.

Moreover, we also investigated the Co_2 pair as a potential catalyst within the context of homonuclear MOF—based DACs. The dual Co atoms were anchored by a Robson—type ligand and subsequently incorporated into the UiO—68 framework, resulting in the Co_2 —MOF(-NH₂) catalyst [33] (Figure 3c).

[[]b] SA: Sacrificial agent.

^[c] TEOA: triethanolamine.

 $^{^{[}d]}$ BIH: 1,3-dimethyl-2-phenyl-2,3-dihydro-1H-benzoimidazole.

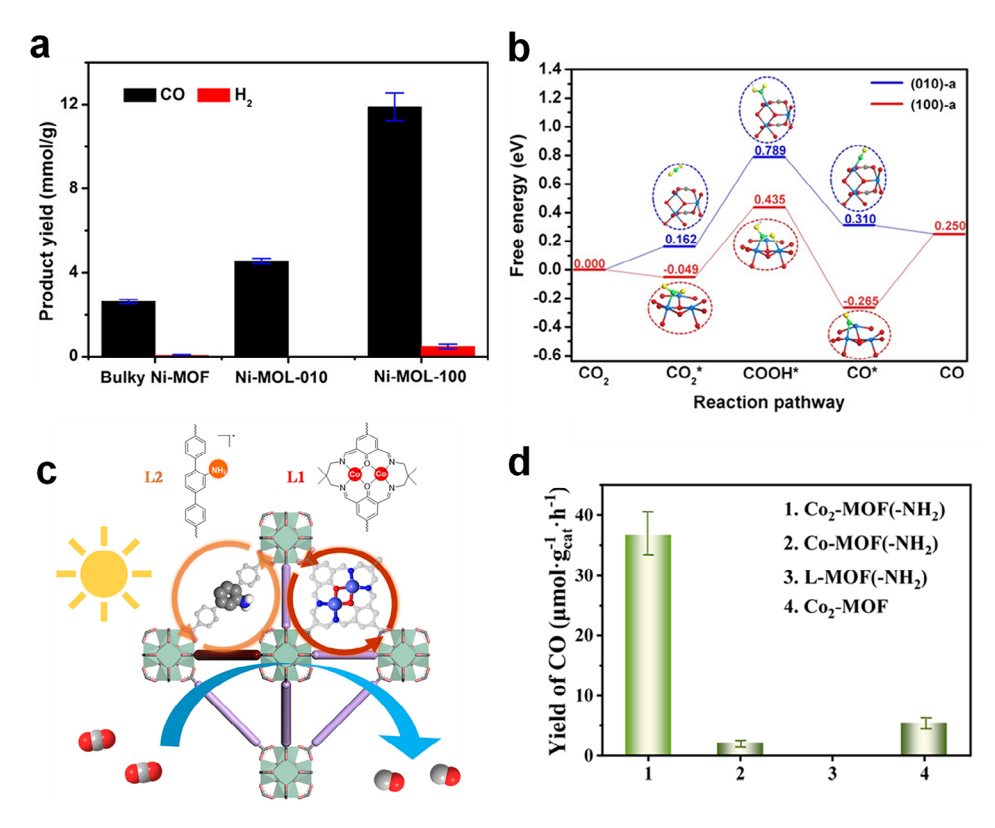


Figure 3. (a) The photocatalytic activities of bulky Ni-MOF, Ni-MOL-010, and Ni-MOL-100. (b) Calculated free energy diagrams for the reduction of CO₂ to CO on the optimized (010) and (100) crystal facets. Reproduced from ref. 28 with permission from Wiley-VCH, Copyright 2021. (c) Schematic illustration of the framework structures and bridging ligands of Co₂-MOF(-NH₂), (d) Comparison of CO production rate of Co₂-MOF(-NH₂), Co-MOF(-NH₂), L-MOF(-NH₂), and Co₂-MOF. Reproduced from ref. 33 with permission from The Royal Society of Chemistry, Copyright 2023.

The photocatalytic CO₂RR reactions were conducted using Co₂-MOF(-NH₂) catalysts in a CO₂-saturated mixture of CH₃CN and H₂O with BIH as a sacrificial reductant (Table 1). The CO yield of Co_2 -MOF(-NH₂) was significantly higher (2.44 mmol $g_{Co}^{-1} h^{-1}$) compared to Co-MOF(-NH₂) (0.23 mmol g_{Co}^{-1} h⁻¹), highlighting the synergistic catalysis effect. The durability test showed that Co₂-MOF(-NH₂) maintained stable CO yields over four runs, with no significant loss in crystallinity or integrity. These results demonstrate the efficient performance and stability of Co₂-MOF(-NH₂) for CO₂ photoreduction. In situ FTIR spectra showed *COOH and *CO intermediates, with *CO formation as the rate-determining step. DFT calculations revealed that Co_2 -MOF(-NH₂) exhibits a lower ΔG for the rate-determining step (1.59 eV) compared to Co-MOF(-NH₂) (1.98 eV) (Figure 3d). The introduction of binuclear Co centers in Co₂-MOF(-NH₂) shifts the d-band center, enhancing *COOH adsorption and improving catalytic activity through a synergistic effect.

Heteronuclear MOF-based DACs: The heteronuclear bimetallic active sites in MOFs can also exhibit synergistic effects to give rise to high photocatalytic activity for the CO₂RR. Zhong et al. successfully incorporated Cu and Ni dual-metal sites into the robust MOF-808, resulting in a bioinspired MOF-808-CuNi photocatalyst for CO_2 -to- CH_4 conversion. [30] When the MOF catalyst lacked metal sites, it exhibited the HCOOH is the main product. However, when Ni species were incorporated into the MOF-808 framework, the main product HCOOH evolution rate showed only a slight decrease. The catalytic performance improved significantly with the incorporation of Cu²⁺. MOF-808-CuNi demonstrated an increased CH₄ production rate of 158.7 $\mu mol\ g^{-1}\ h^{-1}$ and effectively suppressed HCOOH formation (Table 1). To investigate the charge transfer behavior, electron spin resonance (ESR) measurements were conducted. The ESR peak at q = 2.002 corresponds to oxygen-centered active sites in Zr-oxo clusters, where electrons are transferred from [Ru(bpy)₃]Cl₂. Under CO₂, the ESR signals associated with Cu(II) and Ni(I) change, indicating electron migration from Zr-oxo sites to the Cu/Ni dual-metal sites. In situ diffuse reflectance infrared Fourier transform spectroscopy (DRIFTS) reveals that species like HCO₃*, CO₃*, and CO₂* act as potential intermediates for C1 fuel production. Additionally, OCH₃* and CH₃* intermediates are key in the CO₂-to-CH₄ photoreduction process. DFT calculations confirm electron transfer from Zr-oxo clusters to Cu/Ni sites, coupling with CO₂ to produce CH₄. The synergistic effect between Cu and Ni stabilizes C1 intermediates and suppresses byproduct formation, thereby leading to high CH₄ selectivity (Figure 4a). Furthermore, the self-adaptive Cu/Ni dual-metal sites in MOF-808-CuNi play a crucial role in enhancing the photocatalytic CO₂ reduction process. Structural analysis showed that key parameters, such as the Cu-Ni bond distance (d_{Cu-Ni}) and the N-N bond angle, evolve dynamically during the reaction. Initially, the d_{Cu-Ni} distance is 4.312 Å, which adjusts to 4.454 Å upon adsorption of COOH* after the first proton-coupled electron transfer. As COOH* evolves into HCOOH*, the distance further changes to 4.356 Å. The N-N bond

, 28. Downloaded from https://chemistry-ucope.onlinelibinary.wiley.com/doi/10.1002/chem.20250636 by Tainin University Of, Wiley Online Library on [21/10/2025]. See the Terms and Conditions (https://onlinelibrary.wiley.com/terms-and-conditions) on Wiley Online Library for rules of use; OA articles are governed by the applicable Creative Commons Licenses

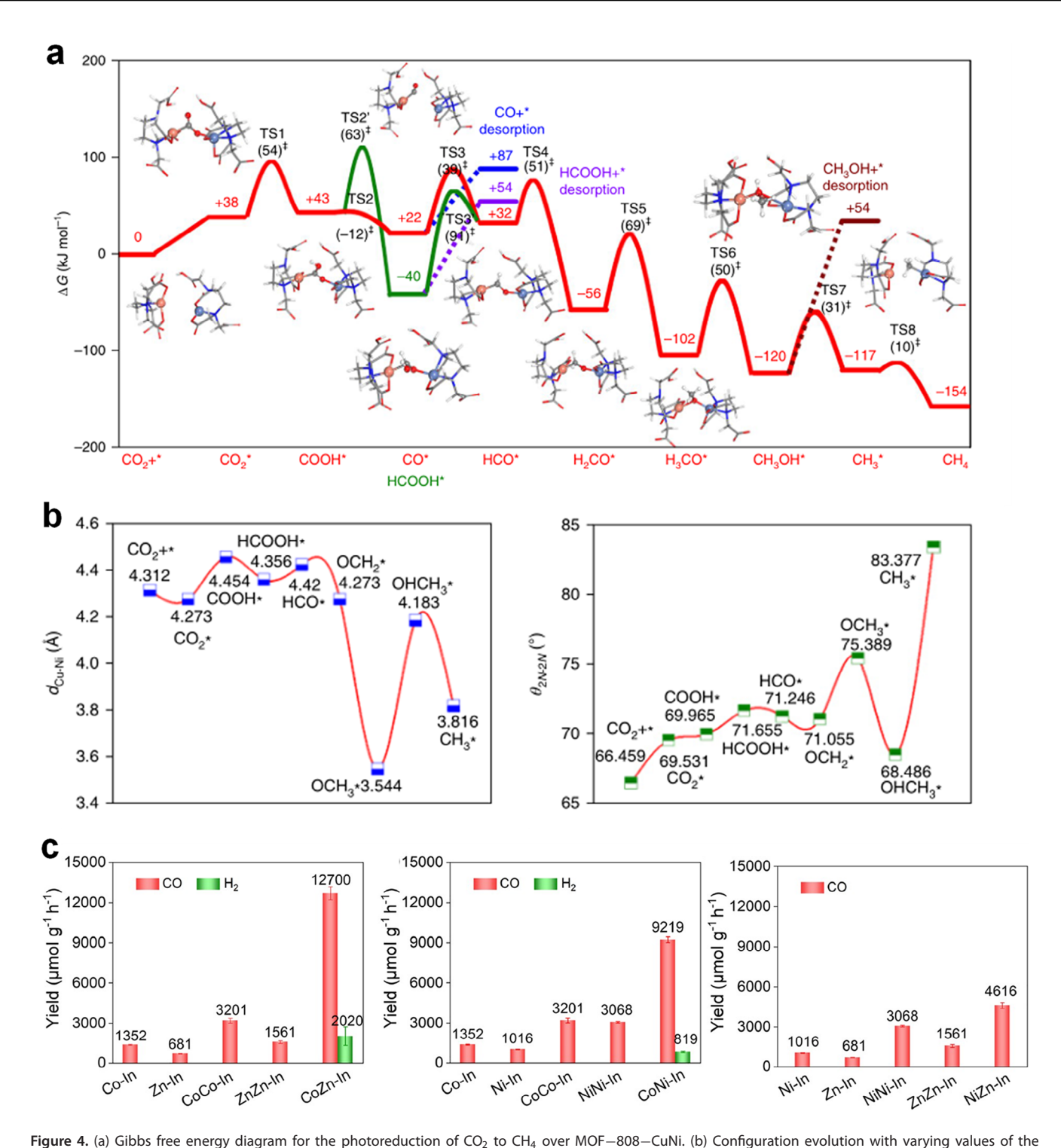


Figure 4. (a) Globs free energy diagram for the photoreduction of CO_2 to CH_4 over MOF—808—CuNi. (b) Configuration evolution with varying values of the Cu—Ni bond distance (d_{Cu-Ni}) and the N—N bond angle. Reproduced from ref. 30 with permission from Springer Nature, Copyright 2024. (c) Photocatalytic CO_2 reduction by CoZn—In, CoNi—In, and NiZn—In, as well as related M—In and MM—In. Reproduced from ref. 31 with permission from Springer Nature, Copyright 2021.

angle also varies from 66.459° to 83.377° during the reaction (Figure 4b). These dynamic adjustments of the Cu/Ni dual—metal sites help stabilize the C1 intermediates and suppress the desorption of byproducts, contributing to the high selectivity for CO_2 reduction to CH_4 .

Furthermore, heteronuclear MOF–based catalysts such as CoZn-In, CoNi-In, and NiZn-In, [31] also have shown significant

improvement in photocatalytic CO_2 reduction compared to their mononuclear counterparts (Figure 4c, Table 1). Notably, CoZn—In exhibited the highest performance, achieving a CO yield of 12,700 μ mol g $^{-1}$ h $^{-1}$, and a quantum yield of 2.05%, which is significantly higher than that of the corresponding monometallic Co—In, Ni—In, and Zn—In as well as homometallic CoCo—In and ZnZn—In catalysts. highlighting its superior

Chemistry Europe

European Chemical Societies Publishing

photoelectric conversion capability. This enhancement is attributed to the DMSC effect, wherein the combination of Co and Zn sites facilitates efficient CO₂ reduction. The DMSC effect was further verified through natural bond orbital (NBO) charge calculations, which indicated that the stronger binding affinity of Zn²⁺ to OH⁻ enhances the cleavage of the C—OH bond in the [O = C-OH] intermediate, thus accelerating the CO₂-to-CO conversion. This synergy between Co and Zn also stabilizes key intermediates, leading to improved selectivity and efficiency. Isotope tracing experiments confirmed that the CO produced originated from CO₂, further supported by control experiments that showed negligible CO production in the absence of catalyst, light, and CO₂. In addition to its high activity, CoZn-In also exhibited excellent stability, maintaining its catalytic performance over at least four reaction cycles. Moreover, the catalyst displayed strong activity under a simulated flue gas environment (10% CO₂ and 90% Ar), demonstrating its potential for practical applications in CO₂ reduction.

Therefore, MOF-based DACs both homonuclear and heteronuclear exhibit significant potential for enhancing photocatalytic CO₂ reduction. The synergistic effects between dual-metal sites, as seen in Ni₂-based, Co₂-based, and Cu-Ni DACs, play a pivotal role in improving catalytic efficiency and selectivity. These interactions often facilitate more efficient charge transfer, stabilize key intermediates, and lower the activation energy required for CO₂ conversion, all of which contribute to their high performance. Notably, heteronuclear systems such as CoZn-In demonstrate outstanding performance, with CO yields substantially higher than their mononuclear counterparts. These properties allow for better control over reaction intermediates and improve the overall selectivity toward desired products. Future research should focus on exploring novel metal combinations, optimizing dynamic coordination environments, and advancing mechanistic understanding to further develop high-performance MOF-based catalysts for sustainable CO₂ reduction.

4. Electrocatalytic CO₂ Reduction

Electrocatalytic CO₂ reduction represents a promising strategy for converting CO₂ into valuable products such as fuels and chemicals.^[34–36] This section examines the role of MOF—based DACs in enhancing the efficiency of this process. Particular attention is given to how the combination of metal pairs within MOFs can improve the selectivity and effectiveness of CO₂ conversion. Furthermore, the challenges associated with catalyst stability and performance in practical applications are addressed. The catalytic performance of various DACs is summarized in Table 2, offering a comprehensive overview of their capabilities.

Homonuclear MOF-based DACs: Liao et al. reported a Cu_2 catalyst, $[Cu_2(obpy)_2]$ (Cuobpy, where Hobpy = 1H-[2,2']bipyridinyl-6-one), a cuprous complex in which each Cu(I) ion adopts a trigonal geometry, coordinated by two nitrogen atoms from one obpy⁻ ligand and one oxygen atom from another.^[37] The Cu(I) ions form a dimeric

structure, with a short intramolecular Cu-Cu distance of 2.58 Å and two interdimer Cu-Cu interactions of 2.99 Å (Figure 5a). In an H-type cell, Cuobpy-SL nanosheets exhibited significantly higher performance at - 1.4 V versus RHE, with a faradaic efficiency (FE) of 82% for CH₄ at a current density of 22 mA cm⁻² (Figure 5b). In a flow-cell device, Cuobpy-SL achieved a current density of approximately 90 mA cm⁻² while maintaining an FE of 82%. Operando ATR-FTIR spectra collected at - 1.4 V versus RHE in CO₂-saturated 0.1 M KHCO₃ revealed key intermediates in the electrocatalysis CO₂RR process, including *COOH, *CHO, *CH₂O, and *CH₃O. DFT calculations indicated that *CO species bridging two Cu ions are favored over single Cu coordination, promoting the formation of *CHO with a lower energy barrier. The confined dicopper sites in Cuobpy—SL hinder C—C coupling, enhancing CH₄ selectivity. These findings highlight the critical role of the dicopper site in stabilizing intermediates and guiding the reaction pathway toward CH₄ production.

Furthermore, they designed MOF-based DAC PcCu-Cu-O, incorporating metallo-ligand (2,3,9,10,16,17,23,24—octahydroxy—phthalocyaninato) copper(II) (PcCu-(OH)₈) to achieve more deeply reduced products, particularly C₂₊ products.^[38] PcCu-Cu-O is a 2D MOF composed of PcCu-(OH)₈ ligands and square-planar CuO₄ nodes (Figure 5c). Compared to discrete molecular copper-phthalocyanine (with an FE of C₂H₄ = 25%), PcCu-Cu-O exhibits significantly improved performance for the electrocatalytic reduction of CO₂ to C₂H₄, achieving an FE of 50(1)%, and a current density of 7.3 mA cm^{-2} at - 1.2 V versus RHE in 0.1 M KHCO₃ solution (Figure 5d). Periodic DFT studies reveal that the two *CO intermediates are separated by 8.95 Å, preventing direct C-Cdimerization into the *OCCOH intermediate, which means that one of the *CO intermediates must desorb before dimerization can occur. The *CO adsorption energy on the CuPc unit is significantly higher (48 kJ mol⁻¹) compared to the CuO₄ unit (16 kJ mol⁻¹), due to differences in the coordination fields around the metal ions. Since the CuO₄ unit is highly active for CO₂ reduction to CO, its lower *CO adsorption energy suggests that it acts as an ideal CO source for C-C dimerization on CuPc during CO₂RR. In contrast, the higher *CO adsorption energy on CuPc favors the hydrogenation of CO to *CHO before dimerization (Figure 5e). Therefore, the combination of CuPc and CuO₄ units in PcCu-Cu-O significantly lowers the energy barrier for C-C dimerization compared to discrete molecular PcCu and PcCu-(OH)₈ catalysts, resulting insuperior performance. In-situ ATR-FTIR measurements were performed to confirm the *COOH, *CHO, and *COCHO intermediate. Most notably, the absorption peaks for the ${}^*CH_2 = intermediate$ (894 cm⁻¹ for C-H bending and 3108 cm⁻¹ for C-H stretching) were observed, confirming the presence of key intermediates in the electrochemical reduction of CO₂ to C₂H₄ (Figure 5e).

Ligand modulation plays a crucial role in regulating the catalytic performance of MOF-based DACs. For instance, Zhang et al. synthesized three MAF-2 catalysts with different functional groups on the organic ligands via the solvothermal reaction of Cu_2O and dialkyl-1,2,4-triazoles: $[\text{Cu}(\text{dmtz})_{0.33}(\text{detz})_{0.67}]$ (MAF-2ME,

Chemistry Europe

European Chemical Societies Publishing

Material	Electrolyte	Type of cell	E Vs RHE	J	Product of FE				
					СО	CH ₄	C ₂ H ₄	C₂H₅OH	Ref.
Cuobpy	0.1 M KHCO₃	H-type	-1.4 V	12 mA cm ⁻²	_	51%	_	_	[37]
. ,	0.1 M KHCO ₃	H-type	-1.4 V	22 mA cm^{-2}	_	82%	_	_	[37]
	0.1 M KHCO ₃	Flow	-1.4 V	\sim 90 mA cm $^{-2}$	_	82%	-	_	
PcCu-Cu-O	0.1 M KHCO ₃	H-type	-1.2 V	$7.3 \ \text{mA} \ \text{cm}^{-2}$	\sim 3%	\sim 12%	50%	_	[38
MAF-2ME	0.1 M KHCO ₃	H-type	-1.1 V	_	\sim 29%	\sim 3%	\sim 38%	_	[39
MAF-2E	0.1 M KHCO ₃	H-type	-1.3 V	$5.7 \ \text{mA} \ \text{cm}^{-2}$	\sim 8%	\sim 17%	\sim 51%	_	[39
MAF-2P	0.1 M KHCO₃	H-type	−1.5 V	5.7 mA cm ⁻²	\sim 3%	\sim 56%	\sim 21%	_	[39
Cu-Pz-H	1.0 M KOH	Flow	-1.0 V	346.46 mA cm ⁻²	23.57%	8.53%	60%	_	[40
Cu-Pz-Cl	1.0 M KOH	Flow	-1.0 V	-	24.81%	21.03%	32.57%	_	[40
Cu-Pz-Br	1.0 M KOH	Flow	-1.0 V	-	25.64%	25.35%	26.79%	_	[40
Cu-Pz-I	1.0 M KOH	Flow	-1.0 V	287.52 mA cm ⁻²	_	52%	16.04%	-	[40
CuSn-HAB	1.0 M KOH	Flow	−0.57 V	68 mA cm ⁻²	_	_	_	56%	[32

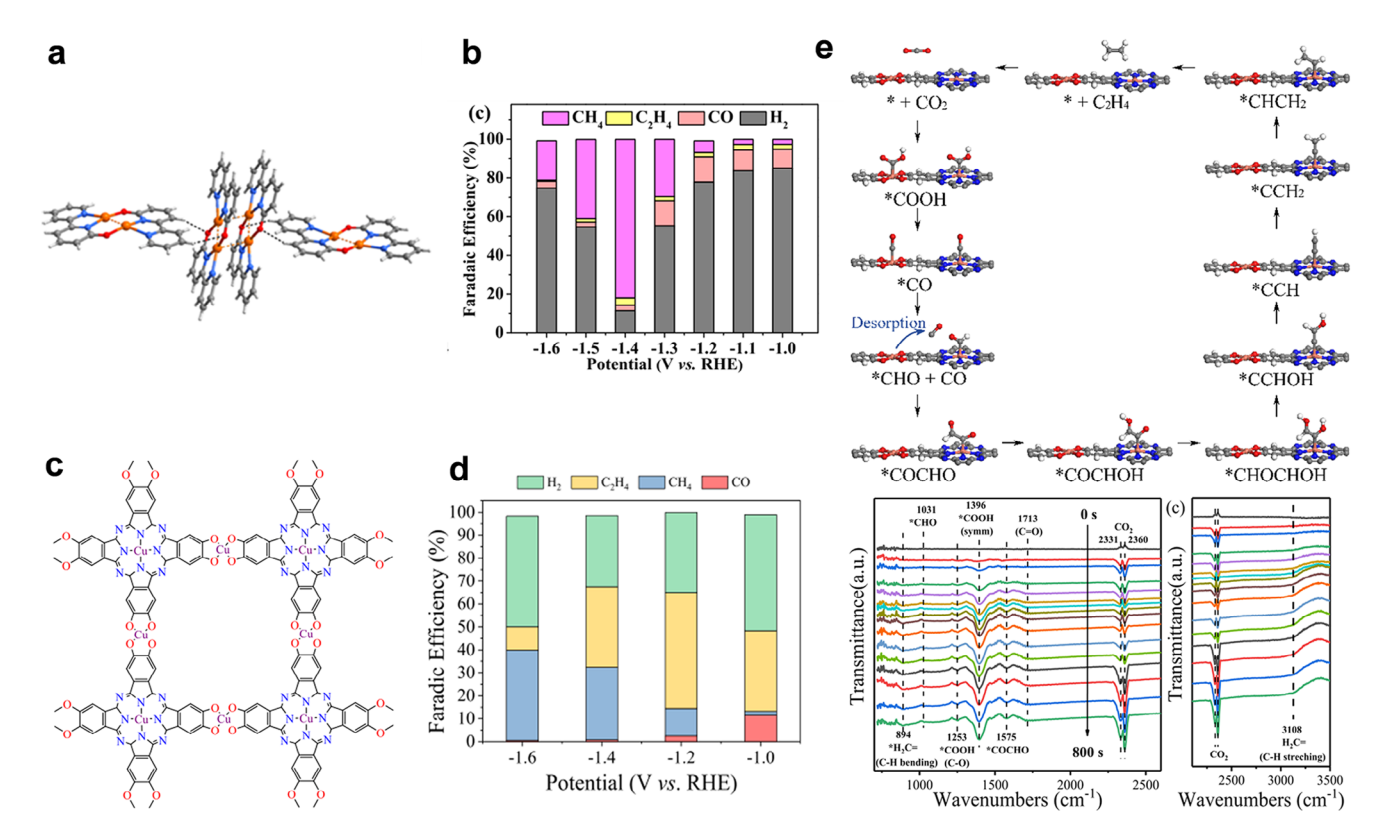


Figure 5. (a) Edge—to—face hydrogen—bonding interactions between adjacent molecules around the dicopper sites of Cuobpy—SL. (b) FEs of different reduced products by Cuobpy—SL as catalysts at different potentials. Reproduced ref. 37 with permission from Copyright 2023, American Chemical Society. (c) Illustration of the structure of PcCu—Cu—O. (d) FEs of C₂H₄, CH₄, CO, and H₂ for PcCu—Cu—O. (e) Proposed CO₂RR mechanism of PcCu—Cu—O and In—situ ATR—FTIR spectra of PcCu—Cu—O during the electrochemical CO₂RR. Reproduced ref. 38 with permission from Copyright 2021, American Chemical Society.

Hdmtz = 3,5-dimethyl-1,2,4-triazole), MAF-2E, and [Cu(dptz)] (MAF-2P, Hdptz = 3,5-dipropyl-1,2,4-triazole). [39] In these compounds, Cu(I) ions are trigonally bridged, forming dimers with a Cu-Cu distance of 3.4 Å. The electrocatalytic CO₂ reduction efficiency and selectivity of MAF-2ME, MAF-2E, and MAF-2P varied with electrolysis potential. As the potential decreased, the FE for CO decreased while FE for CH₄ and C₂H₄

increased. At - 1.5 V, FE $_{(CH^4\ +\ C2H^4)}$ reached 77%, one of the highest values for MOFs and MOF—derived catalysts. MAF—2E achieved the highest FE for C_2H_4 (51.2 \pm 2.3%) at - 1.3 V, while MAF—2P showed the highest FE for CH $_4$ (55.9 \pm 4.3%) at - 1.5 V. At more negative potentials, the FE(C $_2H_4$)/FE(CH $_4$) ratio decreased, with MAF-2P shifting from C_2H_4 to CH $_4$ selectivity. This selectivity inversion is attributed to the bulky propyl

5213765, 20

28, Downloaded from https://chemistry-europe.onlinelibrary.wiley.com/doi/10.1002/chem.202500636 by Tainin University Of, Wiley Online Library on [21/10/2025]. See the Terms and Conditions (https://onlinelibrary.wiley.com/errars-and-conditions) on Wiley Online Library of rules of use; OA articles are governed by the applicable Ceretive Commons Licenses

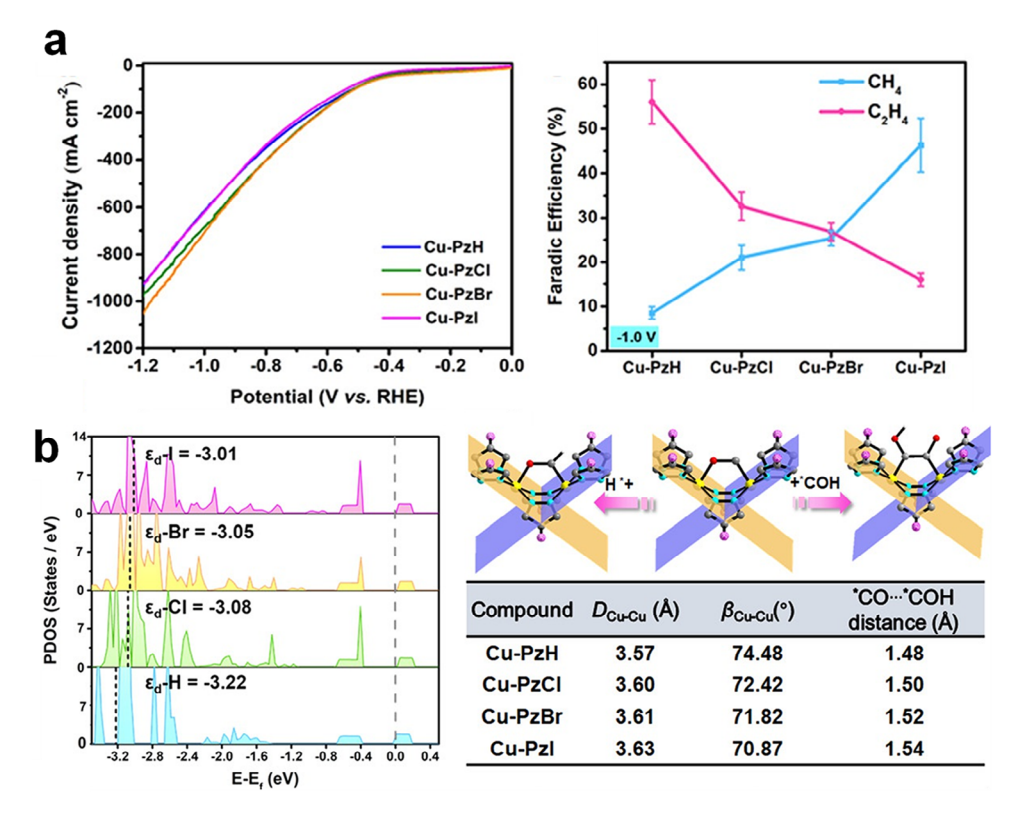


Figure 6. (a) FEs for C_2H_4 on Cu-PzX and FEs for CH_4 on Cu-PzX at different applied potentials. (b) Calculate the partial densities of states (PDOS) of Cu-PzX (X = H, Cl, Br,l) catalysts and the important parameters (D_{Cu-Cu} , β_{Cu-Cu} and the distance of *CO-*COH for C-C coupling) and RDS in the optimized structure of Cu-PzX catalysts. Reproduced from ref. 40 with permission from Wiley-VCH, Copyright 2021.

groups in MAF-2P, which prevent the bi—copper active sites from binding two intermediates simultaneously, promoting CH_4 formation. Theoretical calculations revealed that the coordination geometry of Cu(I) changes from triangular to tetrahedral to accommodate reaction intermediates, with two adjacent Cu(I) ions cooperating for C-C coupling to form C_2H_4 . The ligand side groups regulate catalyst flexibility through steric hindrance, making the C_2H_4 pathway more sensitive than the CH_4 pathway.

In addition, Lan et al. designed and synthesized a series of Cu-based single-chain catalysts (Cu-PzX; X = H, Cl, Br, I; Pz = pyrazole) with different halogen atoms on the pyrazole ligands [40] (Figure 6a). The variations in coordination microenvironment lead to changes in the Cu-Cu distance (from 3.57 to 3.63 Å) and the dihedral angle (from 74.48° to 70.87°), which in turn alter the product distribution during CO_2RR . At -1.0 V versus RHE, Cu-PzH achieves an FE of C₂H₄ of 60%, with a high current density of - 346.46 mA cm⁻², the highest reported for Cu-based crystalline MOF. In contrast, Cu-PzI shows the highest FE for CH₄ (52%) with a partial current density of - 287.52 mA cm⁻² (Figure 6b). Based on the structure models, DFT calculations that Cu–PzH ($D_{\text{Cu-Cu}}=3.57$ Å, $\beta_{\text{Cu-Cu}}=74.48^{\circ}$) has the lowest reaction energy barrier for C2H4 generation because of the shortest *CO···*COH distance (1.483 Å) for C-C coupling. In contrast, Cu-PzI ($D_{Cu-Cu}=3.63$ Å, $\beta_{Cu-Cu}=70.87$ °) is more inclined to the protonation of *CO to produce CH4 with the lowest reaction energy barrier (Figure 6c). The selectivity ratios of CH₄ to C₂H₄ decreased with more negative potentials, highlighting the impact of the coordination microenvironment on product distribution. Based on experimental results and DFT calculations, this selectivity difference can be attributed to two key factors. First, the synergistic effect between neighboring catalytic active sites, induced by changes in the coordination microenvironment, alters the C–C coupling distance. Second, the variation in the coordination microenvironment modifies the adsorption strength of key reaction intermediates by affecting the d–band center of copper, thereby influencing catalytic performance.

Heteronuclear MOF-based DACs: Chen et al. recently developed efficient heteronuclear DACs (CuSn-HAB) featuring unprecedented heterometallic Sn···Cu dual sites, synthesized via a solvothermal method.[32] The catalyst incorporates SnN₂O₂ and CuN₄ coordination, significantly enhancing the efficiency and selectivity of CO2 reduction. Under optimal conditions, CuSn-HAB achieved an FE of 56% for ethanol at - 0.57 V versus RHE, with a current density of 68 mA cm⁻². Additionally, it exhibited impressive reaction rates for ethanol formation, with a partial current density exceeding 38 mA cm⁻² and a turnover frequency of 0.0601 s⁻¹. This performance surpasses that of Cu-HAB, demonstrating the beneficial role of the heterometallic dual sites in facilitating asymmetric C-C coupling. Unlike Cu-based single-site catalysts, which typically lead to competitive product formation, CuSn-HAB exclusively produces ethanol, with no significant generation of other C2+ products. The catalyst displayed excellent stability over 35 hours of continuous operation, with only minor declines in current density and FE, indicating its long-term durability. Operando ATR-FTIR

Europe

doi.org/10.1002/chem.202500636

analysis identified key intermediates, such as *CO, *OCH2, and #CO-*OCH2, which are crucial for ethanol formation. The CuN4 site coordinates with the four nitrogen atoms, while the SnN₂O₂ site, which has a higher oxygen affinity, plays a pivotal role in generating *OCH₂ and promoting *CO-*OCH₂ dimerization for ethanol production. DFT calculations revealed that the low Gibbs free energy for the C-C coupling between these intermediates contributes to the high efficiency of CuSn-HAB. Furthermore, isotope labeling experiments confirmed that the CO in the ethanol product originates from CO₂.

Overall, both homonuclear and heteronuclear MOF-based DACs can significantly enhance electrocatalytic CO₂ reduction activity and selectivity. Highlighted examples, including Cu₂(obpy), PcCu-Cu-O, MAF-2, Cu-PzX, and CuSn-HAB, clearly demonstrate the crucial roles of metal-metal synergy, ligand modification, and precise site engineering for CO₂ reduction. Challenges remain regarding the long-term stability and scalability, as well as the conductivity of MOF-based DACs. Thus, future studies need to focus on optimizing catalyst design to improve the durability and conductivity of MOF-based DACs, and developing comprehensive mechanistic insights to further advance MOF-based DACs toward practical electrocatalytic CO₂ conversion applications.

5. Summary and Outlook

This review presents a comprehensive overview of the recent advancements in MOF-based DACs for photocatalytic and electrocatalytic CO₂RR, focusing on their synthesis strategies, catalytic mechanisms, and applications. DACs, where two metal atoms are precisely incorporated into the support material, exhibit unique advantages over traditional catalysts due to their DMSC effect. This effect enhances reactant activation, accelerates charge transfer, and reduces activation energy, thereby significantly improving the catalytic performance for CO₂RR. The review investigates various approaches for synthesizing MOF-based DACs, highlighting the tunability of MOFs and their ability to host dual-atom sites with high atomic efficiency. These advantages make MOF-based DACs ideal candidates for enhancing the stability, selectivity, and kinetics of CO₂RR. Additionally, the review elaborates on the impact of the local electronic structure, coordination environment, and metal-metal interactions on catalytic performance, providing insights into the mechanisms behind the DMSC effect. Despite the promising potential of MOF-based DACs, several challenges remain. The design and synthesis of these catalysts require precise control over metal site placement, coordination geometry, and stability under reaction conditions, Future research should focus on improving the stability of MOF-based DACs under practical conditions, developing advanced synthesis techniques for precise metal positioning, and investigating the effect of metal-metal distance in MOF-based DACs on CO2 reduction activity and product selectivity. Additionally, a deeper understanding of the structure-performance relationship through advanced in-situ characterization techniques and computational modeling will be crucial for optimizing catalyst design and expanding their applicability in CO₂ reduction.

Acknowledgments

This work was supported by the National Key Research and Development Program of China (2022YFA1502902), and the National Natural Science Foundation of China (22201209).

Conflict of Interests

The authors declare no conflict of interest.

Data Availability Statement

Data sharing is not applicable to this article as no new data were created or analyzed in this study.

Keywords: CO₂ reduction • dual—atom catalysts • electrocatalysis · metal-organic frameworks · photocatalysis

- [1] K. R. Abbasi, M. Shahbaz, J. Zhang, M. Irfan, R. Alvarado, Renewable Energy 2022, 187, 390-402.
- [2] F. Al Mubarak, R. Rezaee, D. Wood, Energy Rev 2024, 5, 1232-1265.
- J. L. Holechek, H. M. E. Geli, M. N. Sawalhah, R. Valdez, Sustainability 2022, 14, 4792.
- [4] A. Al-Shetwi, Sci. Total Environ. 2022, 822, 153645.
- [5] M. Zhang, M. Lu, M. Yang, J. Liao, Y. Liu, H. Yan, J. Chang, T. Yu, S. Li, Y. Lan, eScience 2023, 3, 100116.
- [6] H. H. Wong, M. Sun, T. Wu, C. H. Chan, L. Lu, Q. Lu, B. Chen, B. Huang, eScience 2024, 4, 100140.
- [7] Y. Lei, Z. Wang, A. Bao, X. Tang, X. Huang, H. Yi, S. Zhao, T. Sun, J. Wang, F. Gao, Chem. Eng. J. 2023, 453, 139663.
- [8] C. Vogt, B. Weckhuysen, Nat. Rev. Chem. 2022, 6, 89-111.
- [9] D. Song, Y. Lian, M. Wang, Y. Su, F. Lyu, Z. Deng, Y. Peng, eScience 2023, 3, 100097.
- [10] D. Wang, J. Mao, C. Zhang, J. Zhang, J. Li, Y. Zhang, Y. Zhu, eScience 2023, 3, 100119.
- [11] D. Zhong, Y. Gong, C. Zhang, T. Lu, Chem. Soc. Rev. 2023, 52 3170-3214.
- [12] Y. Cui, C. Ren, Q. Li, C. Ling, J. Wang, J. Am. Chem. Soc. 2024, 146, 15640-15647.
- [13] Š. Kment, A. Bakandritsos, I. Tantis, H. Kmentová, Y. Zuo, O. Henrotte, A. Naldoni, M. Otyepka, R. S. Varma, R. Zbořil, Chem. Rev. 2024, 124, 11767-11847.
- [14] X. Yan, C. Duan, S. Yu, B. Dai, C. Sun, H. Chu, Renew. Sustain. Energy Rev. 2024, 190, 114086.
- [15] N. Farooq, Z. U. Rehman, M. I. Khan, S. Asghar, M. Saleem, R. Irshad, A. Sheikh, A. Shanableh, S. Manzoor, Z. U. Khan, New J. Chem. 2024, 48, 8933-8962.
- [16] S. Vijayaram, H. Razafindralambo, Y. Sun, S. Vasantharaj, H. Ghafarifarsani, S. H. Hoseinifar, M. Raeeszadeh, Biol. Trace Elem. Res. 2024, 202, 360-386.
- [17] Y. Chen, J. Lin, Q. Pan, X. Liu, T. Ma, X. Wang, Angew. Chem. Int. Ed. 2023, 62, e202306469.
- [18] R. Li, D. Wang, Adv. Energy Mater. 2022, 12, 2103564.
- [19] M. Wong, J. J. Foo, J. Y. Loh, W. Ong, Adv. Energy Mater. 2024, 14, 2303281.
- I. Abánades Lázaro, X. Chen, M. Ding, A. Eskandari, D. Fairen-Jimenez, M. Giménez-Marqués, R. Gref, W. Lin, T. Luo, R. S. Forgan, , Nat. Rev. Methods Primers 2024, 4, 42.
- [21] Z. Zheng, H. L. Nguyen, N. Hanikel, K. K. Li, Z. Zhou, T. Ma, O. M. Yaghi, Nat. Protoc. 2023, 18, 136-156.

- m.202500636

 Chemistry
 Europe

 European Chemical
 Societies Publishing
- [22] W. Gong, Z. Chen, J. Dong, Y. Liu, Y. Cui, Chem. Rev. 2022, 122 9078-9144.
- [23] Z. Han, Y. Yang, J. Rushlow, R. Liang, H. Zhou, Acc. Chem. Res. 2024, 57, 3217-3226.
- [24] X. Mu, M. Yu, X. Liu, Y. Liao, F. Chen, H. Pan, Z. Chen, S. Liu, D. Wang, S. Mu, ACS Energy Lett. 2024, 9, 5763-5770.
- [25] X. Zhang, C. Gao, L. Li, X. Yan, N. Zhang, B. Junjiang., J. Colloid Interface Sci. 2024, 676, 871-883.
- [26] J. Liu, S. Zhao, C. Wang, B. Hu, L. He, M. Wang, Z. Zhang, M. Du, Adv. Mater. Interfaces 2022, 9, 2200913.
- [27] Z. Yan, M. Du, J. Liu, S. Jin, C. Wang, G. L. Zhuang, X. J. Kong, L. S. Long, L. S. Zheng., *Nat. Commun.* 2018, 9, 3353.
- [28] W. Yang, H. Wang, R. Liu, J. W. Wang, C. Zhang, C. Li, D. C. Zhong, T. B. Lu., Angew. Chem. Int. Ed. 2021, 60, 409-414.
- [29] H. Liang, R. Liu, C. Hu, X. An, X. Zhang, H Liu, J Qu., J. Hazard. Mater. 2021, 406, 124692.
- [30] J. Li, H. Huang, W. Xue, K. Sun, X. Song, C. Wu, L. Nie, Y. Li, C. Liu, Y. Pan, H.-L. Jiang , D. Mei, C. Zhong, Nat. Catal. 2021, 4, 719-729.
- [31] H. Wang, W. Shi, Y. Yang, B.-X. Dong, T.-B. Lu, D.-C. Zhong, Sci. China Chem. 2025, 68, 201-208.
- [32] Z. Zhao, J. Huang, P. Liao, X. M. Chen., J. Am. Chem. Soc. 2023, 145, 26783-26790.

- [33] M. Ming, Y. Wang, W. Tao, W.-J. Shi, D.-C. Zhong, T.-B. Lu, Green Chem. 2023, 25, 6207-6211.
- [34] M. Huang, S. Zhou, C. Yang, C. Dong, Y. He, W. Wei, X. Li, Q. Zhu, Z. Huang, ACS Nano 2024, 18, 33210-33219.
- [35] L. Jiao, X. Li, W. Wei, S. Zhou, S. Han, D. Ma, Y. Mao, Q. Xu, X. Wu, Q. Zhu, Appl. Catal. B Environ. 2023, 330, 122638.
- [36] S. Wang, X. Yuan, S. Zhou, X. Li, S. Han, W. Lin, L. Zheng, D. Ma, Q. Zhu, Energy Mater 2024, 4, 400032.
- [37] J. Heng, H. Zhu, Z. Zhao, C. Yu, P. Liao, X. Chen, J. Am. Chem. Soc. 2023, 145, 21672-21678.
- [38] X. Qiu, H. Zhu, J. Huang, P. Liao, X. Chen, J. Am. Chem. Soc. 2021, 143, 7242-7246.
- [39] L. Zhuo, P. Chen, K. Zheng, X. Zhang, J. Wu, D. Lin, S. Liu, Z. Wang, J. Liu, D. Zhou, J. Zhang, Angew. Chem. Int. Ed. 2022, 61, e202204967.
- [40] R. Wang, J. Liu, Q. Huang, L. Dong, S. Li, Y. Lan, Angew. Chem. Int. Ed. 2021, 60, 19829-19835.

Manuscript received: February 18, 2025 Revised manuscript received: March 27, 2025 Version of record online: April 26, 2025